Available online at www.sciencedirect.com
SCIENCE DIRECT
ELSEVIER
polymer
Polymer 46 (2005) 2404–2417
www.elsevier.com/locate/polymer

Stochastic simulation of thin photoresist film dissolution: a dynamic and a quasi-static dissolution algorithm for the simulation of surface and line-edge roughness formation

G.P. Patsis*

Institute of Microelectronics, NCSR Demokritos, Aghia Paraskevi, Attiki, Athens 153-10, Greece

Received 4 November 2004; received in revised form 3 January 2005; accepted 3 January 2005

Abstract

Stochastic simulation techniques gain increased importance in the field of microelectronic processes especially since the sub-100 nm device dimensions have been reached. In this work, stochastic Monte Carlo techniques are incorporated to simulate photoresist polymer chains in a lattice, while all the phenomena taking place during film dissolution are considered in terms of occurrence probabilities in order to describe the dynamics of dissolution. Chain removal is based on the critical ionization fraction criterion. The exponential decrease of dissolution rate with increasing polymerization length is proven and its relation to critical ionization is investigated both in two and three dimensions (2D/3D), resulting in an efficient method for the determination of the dissolution rate in terms of polymerization length and critical ionization fraction. While the dynamic dissolution algorithm is appropriate for obtaining information about dissolution rate and surface roughness evolution, the increased computational time in high values of critical ionization fraction and lattice sizes, especially in 3D, make it inappropriate for line-edge roughness studies. A quasi-static 2D/3D resist dissolution algorithm, which is free of the dissolution blocking problems and orders of magnitude faster than the dynamic one, based again on the critical ionization criterion, is constructed in order to reliably quantify line-edge roughness.
© 2005 Elsevier Ltd. All rights reserved.

PACS: 85.40.Hp; 85.40.Ux

Keywords: Polymer science and technology; Polymer dissolution; Lattice models of polymer chains

1. Introduction

In the last few years, the microelectronics research has entered dynamically in the area of sub-100 nm device fabrication. Research in these dimensions had already a long time ago foreseen the problems originating from the nonuniformity of the sidewalls of the created structure. These were attributed to either process or material. The term used to describe the quantity of non-uniformity of sidewalls of the micro-nano structure is line-edge roughness (LER) or sidewall roughness and of the surface, surface-roughness (SR). By roughness in the following we mean the root-mean-square (rms) deviation (1 sigma or 3 sigma) of the profile shape from the straight line (2D) or plane (3D). The 3-sigma value is used, because in most cases the deviation distribution is Gaussian. However, 3 sigma is not enough to completely characterize roughness, and one has also to know the roughness exponent and the correlation length to describe the high frequency and the spatial variation of roughness [1–3]. In this paper, we will be concerned only with 3 sigma, while we have recently shown that our simulation can also reproduce the other two roughness parameters as well as the dependence of 3 sigma on the edge length [4].

Fig. 1(a) explains the definitions of LER in 3D, while Fig. 1(b) in 2D simulations. Although 3D simulations represent the actual LER definition, what is really measured in experiments with an SEM resembles more the picture

* Tel.: +30 210 6503116; fax: +30 210 6511723.
E-mail address: gpatsis@imel.demokritos.gr.

0032-3861/$ - see front matter © 2005 Elsevier Ltd. All rights reserved.
doi:10.1016/j.polymer.2005.01.049

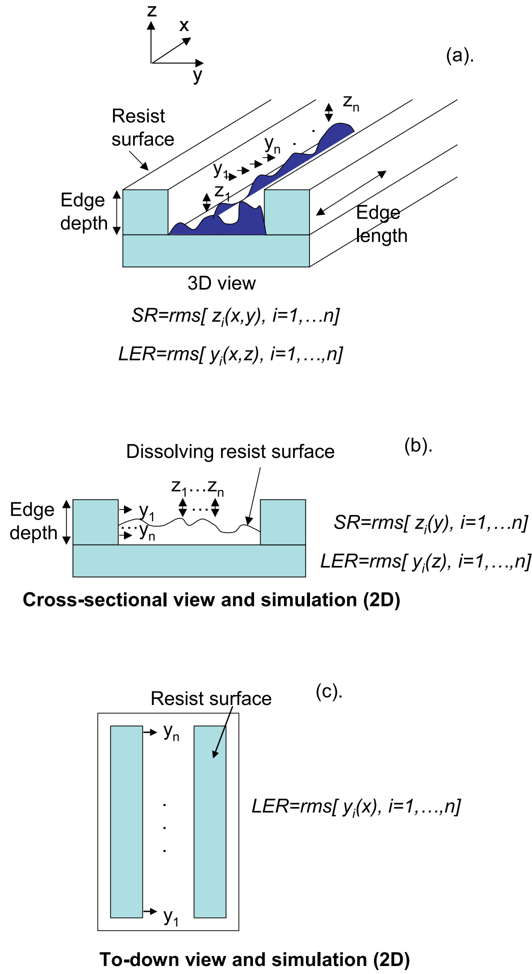

Fig. 1. Definition of surface roughness (SR), and line-edge roughness (LER). Their definition in (a) 3D simulations. (b) 2D simulations—cross-sectional view. (c) 2D simulation top-down view. SR is obtained with the standard dissolution algorithm (SLOW) described in this article, only in cases (a) and (b). The use of the FAST dissolution algorithm loses the SR evolution information but gives faster the LER information in all three kinds of simulation domains.

shown in Fig. 1(c), showing the top-down view of the simulation domain. If N_x, N_y and N_z are the number of sampled points on the edges of the structure on the x-, y- and z-direction, respectively, SR and LER, in 3D (Fig. 1(a)) are defined through the following formulas:

$$\mathrm{SR} = 3\sqrt{\frac{1}{(N_x-1)(N_y-1)}\sum_{i=1}^{N_x}\sum_{j=1}^{N_y}(z_{i,j}-\bar{z})^2}, \tag{1}$$

$$\mathrm{LER} = 3\sqrt{\frac{1}{(N_x-1)(N_z-1)}\sum_{i=1}^{N_x}\sum_{k=1}^{N_z}(y_{i,k}-\bar{y})^2}, \tag{2}$$

where

$$\bar{z} = \frac{1}{N_xN_y}\sum_{i=1}^{N_x}\sum_{j=1}^{N_y}z_{i,j}, \quad \bar{y} = \frac{1}{N_xN_z}\sum_{i=1}^{N_x}\sum_{k=1}^{N_z}z_{i,k}, \tag{3}$$

in the case of 2D simulations (Fig. 1(b)) one of the horizontal dimensions (e.g. the x-direction) is lost, so the corresponding definitions for SR and LER are given as:

$$\mathrm{SR} = 3\sqrt{\frac{1}{(N_y-1)}\sum_{j=1}^{N_y}(z_j-\bar{z})^2}, \tag{4}$$

$$\mathrm{LER} = 3\sqrt{\frac{1}{(N_z-1)}\sum_{k=1}^{N_z}(y_k-\bar{y})^2}, \tag{5}$$

where

$$\bar{z} = \frac{1}{N_y}\sum_{j=1}^{N_y}z_j, \quad \bar{y} = \frac{1}{N_z}\sum_{k=1}^{N_z}y_k. \tag{6}$$

Finally, when simulating the top-down images of photopolymer lines viewed through an SEM (Fig. 1(c)), there is no information on SR, while the definition of LER is:

$$\mathrm{LER} = 3\sqrt{\frac{1}{(N_x-1)}\sum_{i=1}^{N_x}(y_i-\bar{y})^2}, \tag{7}$$

where

$$\bar{y} = \frac{1}{N_x}\sum_{i=1}^{N_x}y_i. \tag{8}$$

Many experimental measurements of surface roughness in resist materials have clarified its dependence on exposure dose, polymer chemical structure, the degree of constituent mixing, the variation of photo-chemical events due to shot noise, the quality of the mask and of the latent image, the solvent–polymer interactions, the polymer and the solvent molecular weight, and the acid diffusion range. The polymer material itself in terms of monomer size, chain stiffness, glass transition temperature, greatly affects roughness also through the control of the mobility of the acid. In addition, the percentage of remaining solvent can affect the acid diffusion and, therefore, LER. Finally the effect of LER on device operation has been examined [5,6].

The effects of the dissolution process are still not clarified completely due to the different models adopted based on the specific material properties. Therefore, the purpose of the current work, is to present a dissolution model capable of quantifying in detail LER and edge position of lithographically determined structures, in terms of polymerization length and acid diffusion range. In this study, the simulation of positive tone resists is performed following previous work in negative tone resists [7]. It considers both two and three-dimensional simulations (2D and 3D, respectively).

The physics of the current dissolution model is based on the critical ionization model [8–10]. According to this model, a polymer chain on the resist film surface in contact with the developer is dissolved only if the fraction of its

ionized monomers to its total number of monomers is equal to or greater than a certain value (the critical ionization fraction, F_C), which is specific for each polymer formulation.

This article is organized as follows: in Section 2 the simulator structure is presented. Section 3 concentrates on the dynamic dissolution module of the algorithm and simulates the dissolution rates of polydisperse and mono-disperse linear chains in 2D and 3D lattices using the critical ionization model. Section 4 investigates the use of the fast quasi-static version of the dissolution algorithm. Finally, Section 5 considers the effects of polymerization length, and acid diffusion range on LER and edge-position using the fast quasi-static dissolution algorithm.

2. General description of the simulation flow

The main focus of the analysis here concentrates on dissolution of the resist and the revelation of the sidewall profile of the resist line. However, all the lithographic steps before development could be simulated, for a complete understanding of roughness evolution through the various lithographic steps. The advantage of the current simulator is its ability to decompose the lithographic process into separate steps and, therefore, it is capable of predicting the effects of each process alone on the final result, either dissolution rate, or roughness. The interesting results of the simulation from the technological importance point of view include the resist-dissolution-rate, R, the surface-roughness

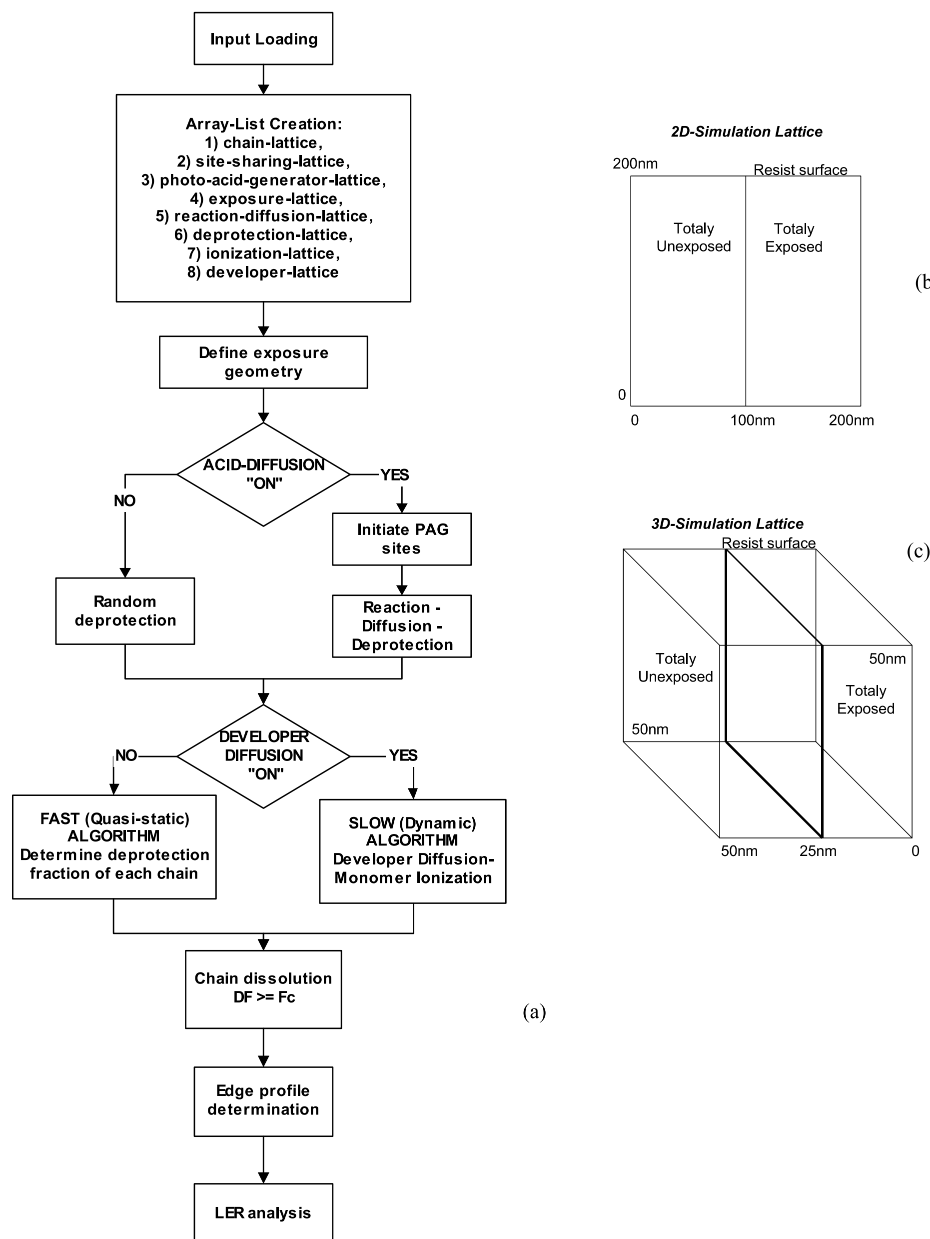

Fig. 2. (a) General view of the simulation flow. (b) 2D simulation lattice structure. (c) 3D simulation lattice structure.

(SR), and line-edge-roughness (LER) in terms of the input parameters.

The simulated processes are quite complex and interdependent and in order to distinguish them, several 'lattice-instances' are used which 'transport' information during execution time. Each 'lattice-instance' represents different aspects of the material during the whole lithography process. Specifically, the simulator manages the information exchange between the following lattice-instances, which in order of creation are: chain-lattice, site-sharing-lattice, photo-acid-generator-lattice, exposure-lattice, reaction-diffusion-lattice, deprotection-lattice, ionization-lattice and finally developer-lattice. All the lattice instances are in 1–1 correspondence regarding their lattice positions. This means that the algorithm has to check before an event if certain constraints are satisfied in each lattice. The corresponding instances are updated during the simulation each time a relevant event happens. Periodic-boundary-conditions were used during chain insertion, only in the horizontal dimensions of the lattice (length and width). In the vertical dimension (height), a reversal in bond direction is done each time a monomer is about to extend the lattice limits over the surface or the bottom, during the chain insertion when the chain lattice is created.

Polymer solubility is simulated by varying the value of F_C. Higher values correspond to more difficultly dissolved polymers.

The general simulation flow is shown in Fig. 2(a). The lattice is orthogonal (i.e. square in 2D and cube in 3D) with a lattice constant equal to 1 nm. The real lattice size should be determined in terms of polymerization length and polymer density for a specific system. Thus, the reported values in nm, are in fact in units of lattice size. Fig. 2(b) shows a sample 2D lattice, half of which is considered exposed to radiation. The analogous 3D case is shown in Fig. 2(c). Polymer chains that are linear self-avoiding and

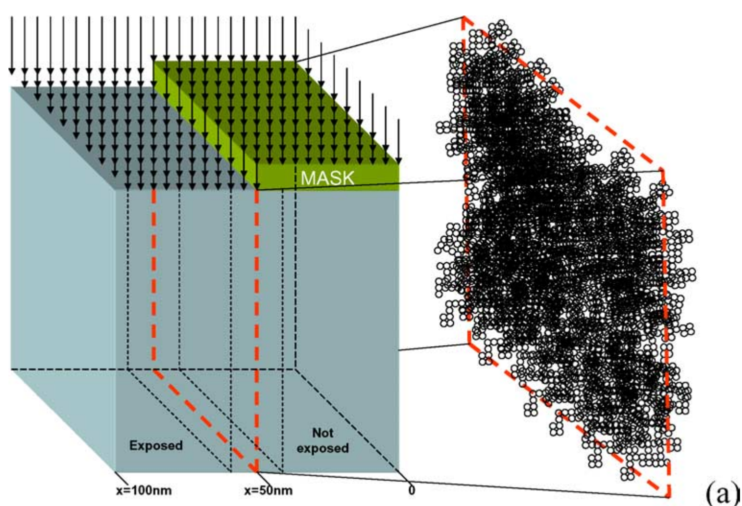

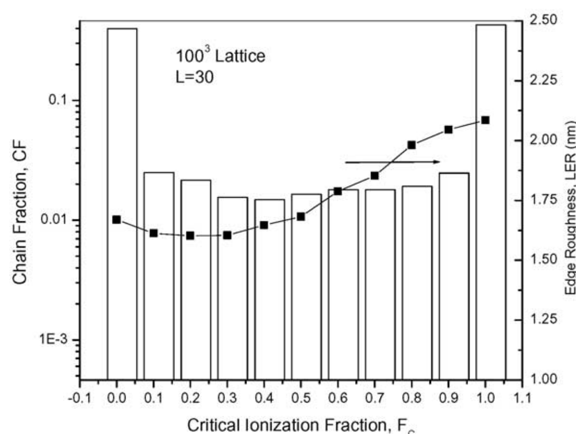

Fig. 3. (a) Qualitative picture of the simulation lattice and of the concept of concentrating on the chains that define the edge, in order to construct the FAST algorithm. (b) Distribution of chain fraction for the values of F_C across the profile edge. The corresponding values of LER when the chains over a certain F_C are removed are shown in the right y-axis. All the monomers in the exposure region are assumed as deprotected in this simulation.

mutually excluded random walks are used to fill the lattice leaving approximately 10% free volume. The characteristics of the chain insertion method has been described in [11]. The polymerization length per chain could be constant (monodisperse chains) or follow a Poisson distribution (polydisperse chains). The resist considered here is chemically amplified and of positive tone, i.e. exposure makes the resist more soluble than it is part not exposed to radiation. The aerial image from exposure is assumed as ideal sharp square wave (Aerial Image Contrast = 1), making all the monomers in the exposure region deprotected (i.e. capable of being ionized by the developer molecules) as is shown in Fig. 2(b) and (c). Extension to non-ideal exposure profiles may be incorporated with suitable transformation of an exposure energy profile from a commercial software package such as PROLITH or SOLID, to acid-generator (PAG) initiation probability.

We can examine the effect of diffusion on LER either by considering acid-diffusion 'on' or 'off'. In the case of considering 'acid-diffusion off', all monomers in the exposure region were set to derpotected state according to a given probability, which is equal to the desired deprotection fraction in the exposed region. This way one is able to determine the sole effect of deprotection fraction on the average edge position and LER without the effect of acid diffusion species, i.e. for a non-chemically amplified resist receiving the necessary dose in order to get the desired deprotection fraction. The term deprtotection fraction DF is used to describe the ratio of the deprotected monomers in the exposed polymer chain lattice with respect to the total number of monomers in the same lattice. The linked list structure of the polymer chain representation in the current algorithm allows for chain-by-chain identification and, therefore, for the exact knowledge of the deprotection/ionization fraction of each chain for each global deprotection fraction. In the current work this was done by simply allowing the algorithm to ask for each monomer site in the polymer chain lattice if it will be deprotected or not. The probability for affirmative answer was in each case the global deprotection fraction. Thus, for example, when DF = 0.3, the 30% of the monomers in the exposed lattice will be deprotected and their distribution was random. In 'diffusion-on' acid diffusion was considered explicitly as the mechanism of deprotection generation.

Accordingly, dissolution algorithm assumes two versions. The SLOW (dynamic) one and the FAST (quasi-static) one. In the dynamic version, dissolution proceeds in dissolution cycles (DC). In each DC, the algorithm identifies the chains that have some of their monomers in contact with the developer. Ionizations are performed on the deprotected monomers. Then the algorithm identifies all those chains with ionization fraction greater than or equal to the critical ionization fraction F_C, and removes them from the lattice. The average thickness and the SR are determined and a new DC starts. The dynamic dissolution algorithm needs to be modified because it takes a lot of CPU time to dissolve the chains, especially in 3D lattices, in order to reveal the sidewall. In the FAST (quasi-static) dissolution version, it is recognized from the beginning of the simulation that the edge profile should be composed of the polymer chains attached to the side that did not satisfy the critical ionization fraction criterion (Fig. 3(a)), i.e. the number of ionized monomers per chain was less then the nominal threshold value for dissolution. Let's consider the geometry shown in Fig. 3(a). The nominal edge position is at $x = 50$ nm and from this point until 100 nm, the monomers in the (50-by-100^2) nm^3 sub-lattice are deprotected (i.e. an ideal square wave exposure destroyed their protecting groups and has made them capable for ionization in the base solution of the developer, and therefore, dissolvable). Then, for a certain critical ionization fraction, F_C, given enough dissolution time, the part on the left would be dissolved and the sidewall (the slice area marked by the dashed lines) would be revealed. The idea is not to wait for the dissolution in terms of monomer ionization-developer diffusion-chain removal cycles, but go directly to the chains in this slice and determine for each one of them its deprotection fraction. The basic assumption made at this point is that given sufficient dissolution time the ionization fraction of a specific chain is going to be equal to its deprotection fraction. If, for example, the slice is taken from 40 to 60 nm, the corresponding distribution of the deprotection fraction of the chains in this slice is shown in Fig. 3(b). The horizontal axis, termed critical ionization fraction, is in fact the deprotection fraction (since ionization probability is assumed $P_{ION} = 1$). Chains with DF = 0, correspond to totally protected ones, while these with DF = 1 to totally deprotected. Therefore, the value of the critical ionization F_C fraction sets a limit in the horizontal axis of this graph in such a way such as, all the chains with DF $\geq F_C$, are dissolved. Then, one needs to determine the resulting LER from the remaining chains. This calculation is orders of magnitude faster than letting the standard dissolution algorithm dissolve the whole left part of the cube. In fact in the right y-axis of Fig. 3(b) the values of the calculated LER are shown, assuming all monomers in the exposure lattice are deprotected. In this example the lattice has been filled with monodisperse chains of polymerization length $L = 30$ and free volume was 10%. For $F_C = 0$ the LER value is the roughness of an arbitrary slice in the non-exposed region. In fact this plot is constructed with the modified dissolution algorithm in less than 2 s on a Pentium IV 3.06 GHs laptop PC with 1 GB RAM.

3. SLOW (dynamic) dissolution algorithm

First, both 2D and 3D simulation were done using the dynamic version of the dissolution algorithm. The following lattice characteristics were used: in 2D a 200 m × 200 nm (200 nm width and 200 nm height) rectangular lattice is

considered (Fig. 2(a)), while in 3D a 50^3 nm^3 cube (Fig. 2(b)).

In all cases the lattice was filled with chains so as to obtain just less than 10% free volume, in each polymerization length. Twenty percent free volume was also tested in 2D simulations with the dynamic algorithm but not marked difference in dissolution rate was recorded, thus no such results are presented. All monomers located in the exposure sub-lattice were considered as deprotected. Thus, the effect of acid diffusion is not present (acid diffusion-'off'), and only the material aspects on dissolution rate and roughness can be evaluated.

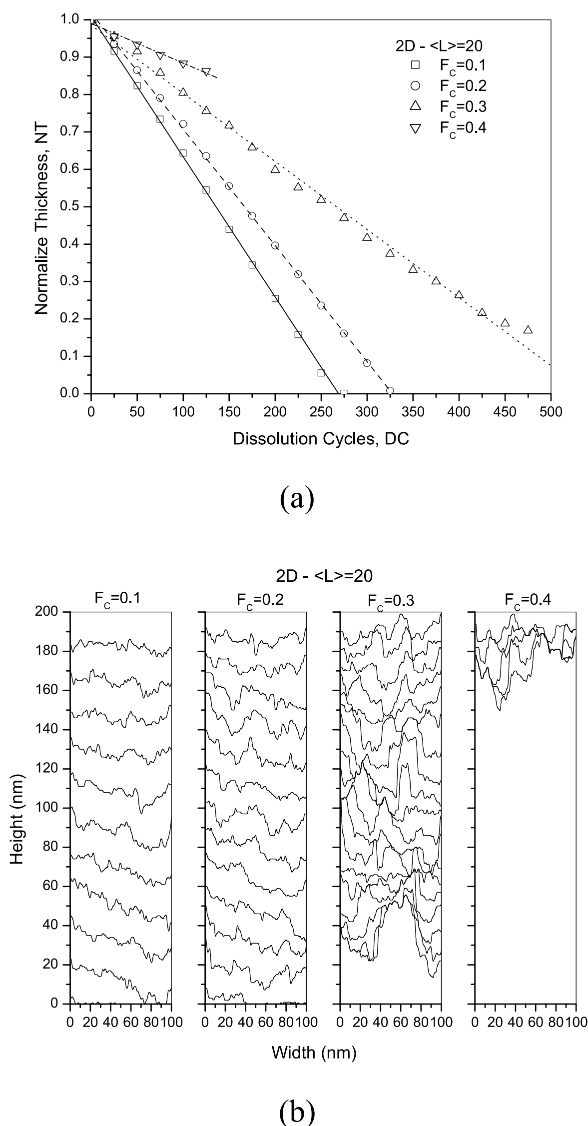

Fig. 4. (a) Normalized thickness (NT) vs. dissolution cycles (DC) from 2D simulation of $\langle L\rangle=20$ chains from a Poisson distribution and critical ionization fraction $F_C=0.1$, 0.2, 0.3 and 0.4. A DC is the CPU time needed by the algorithm to complete the ionization of polymer chains in contact with the developer molecules, find these chains that satisfy the critical ionization fraction criterion, and remove them from the lattice. The total number of DCs necessary for dissolving a specific resist thickness depends upon the lattice size simulated, the polymerization length, and the value of F_C. It can be calibrated to real time (i.e. seconds), when experimental data of NT vs. time (s) for the simulated polymer film are used, by equating the total number of DCs, N_{DC}, to the total dissolution time, t: $N_{DC}=t \Leftrightarrow 1\mathrm{DC}=(t/N_{DC})$ s. Dissolution blocking for $F_C=0.3$ and 0.4 is observed and is a 2D simulation artifact observed also in other simulation works [9]. (b) The corresponding surface profiles. Surface roughness increases with increasing F_C and dissolution blocking. The slope of the surfaces on the right is higher than the left side due to the fact that an un-exposed lattice exists on the left (see Fig. 2(b)). Free volume = 10%. The results are from one simulation.

An example of normalized thickness (NT) vs. dissolution cycles DC is shown in Fig. 4(a) from 2D simulation of polydisperse chains of $\langle L\rangle=20$ average polymerization length. Dissolution is blocked after 80% thickness loss for $F_C=0.3$ and after 20% for $F_C=0.4$. This is a 2D simulation artifact observed also by others [9]. However, it is possible to obtain the linear fits from these data, i.e. the dissolution rate R. The corresponding surface profiles are shown in Fig. 4(b). Increasing surface roughness SR is observed with increasing F_C i.e. with polymer chains with increased dissolution difficulty.

The dissolution rate R obtained from the NT vs. DC graphs in each polymerization length and in each F_C it was found that is linearly decreasing with increasing critical ionization fraction. This was observed either for monodisperse or polydisperse chains and both in 2D and 3D simulations. In fact it was possible to obtain the linear fit expression for each polymerization length. These are shown in Fig. 5(a) for 2D, and in Fig. 5(b) for 3D polydisperse chains. In 2D, dissolution practically stops above $F_C=0.5$, while in 3D it continues until $F_C=0.8$. However, a comparison between 2D and 3D is not easy since neither the width nor the length of the lattice are comparable, nor the number of chains in each lattice. Of course it is clear that in 2D, dissolution blocking is expected to be more pronounced due to limited accessing paths for the developer molecules in the interior of the polymer lattice. The $R(F_C)$ expression with the $\langle L\rangle$ as a parameter can also be used to create the graphs of R vs. $\langle L\rangle$ with F_C as a parameter, shown in Fig. 5(c) for 2D, and in Fig. 5(d) for 3D polydisperse chains. Similar graphs hold for monodisperse chains with slightly different coefficients in the relations of $R(F_C)$ and $R(\langle L\rangle)$. The negative values adjacent to each data series are the slopes of the linear fits. In some cases the fits are obtained only from two points (i.e. for $\langle L\rangle=5$ and 10 monomers per chain) because for higher polymerization lengths the dissolution rate is extremely small, practically zero. The absolute of these values is the exponent n in the $R\sim L^{-n}$ relation implied by these fits. This behavior repeats the observation of Burns et al. [9] that with a single parameter model (F_C) it is possible to describe the dissolution rate behavior with the increase of polymerization length. This was also verified in 2D by performing the same analysis also for 20% free volume. The rates were almost the same (with a slight increase), establishing the characteristic of the model, that the rate-limiting step is the chain ionization and not the developer diffusion in the lattice.

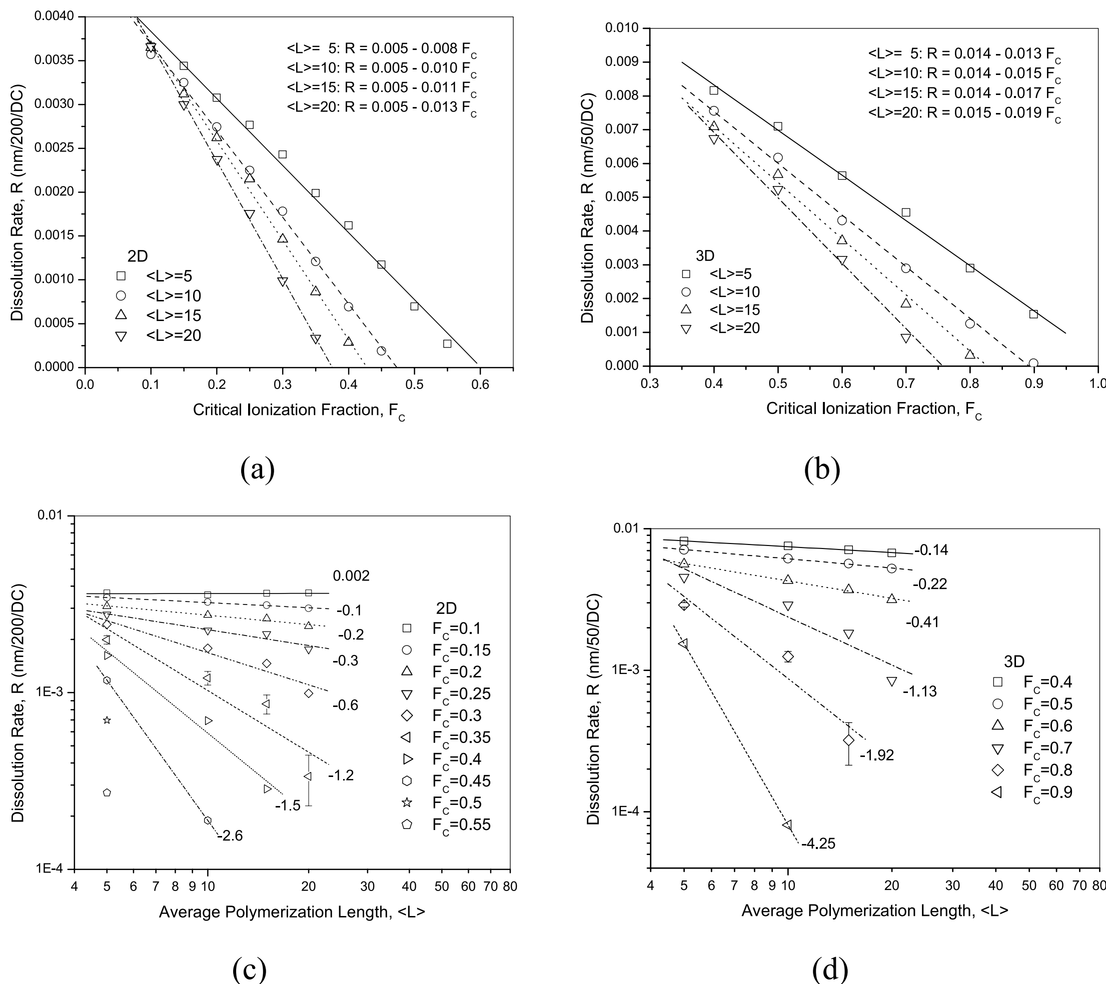

Fig. 5. Dissolution rate R vs. critical ionization fraction F_C for (a) 2D. (b) 3D. Dissolution rate R vs. average polymerization length $\langle L\rangle$ for (c) 2D and (d) 3D. For $F_C=0.5$, and 0.55, only in the $\langle L\rangle=5$ case it was possible to obtain a dissolution rate. Free volume $=10\%$. Each point is the result for 5 averaged simulations.

The exponential decrease of R with polymerization length is reproduced in both 2D and 3D simulations in accordance with the experimental data [9]. However, the slopes from these graphs show different behavior with F_C in 2D and 3D. This is shown in Fig. 6. The monodisperse chains case shows similar $n(F_C)$ behavior as the polydisperse chains. However, the values of n are higher for the same F_C, compared with the polydisperse case, because in the later case it is possible to find for a certain F_C, chains that dissolve since they are shorter and, therefore, more easily satisfy the dissolution criterion. For the cases of polydisperse chains, which are of the more practical interest, the exponential fit functional form is also shown in the graph. The corresponding exponents resulting from the simulations performed in [9] show similar functional behavior, with the exception that it is shifted into lower values of critical ionization fraction and showing steeper increase. This is attributed to the difference of the chain insertion algorithm used in their work (which resembles the full-site sharing chain insertion algorithm [11]) and in the current one (which uses the limited-site sharing chain insertion algorithm [11]).

In fact 3D simulations in the same lattice placing the chains with the full-sharing algorithm [11], reveals the qualitative agreement with Burns et al. simulations. However, in the current implementation of the chain placement algorithm there are some differences in the counting of monomers belonging in shared sites in the lattice in comparison with the chain insertion algorithm used in [8,9]. These result in higher values for the exponent n, meaning more difficult dissolution with polymerization length increase for the same average polymerization length.

Naturally, the value of n is determined from experimental data for a given polymer and developer. Knowing n one can then use the relation $n(F_C)$ to find F_C for the particular polymer-developer combination. This is shown in Fig. 7 where the obtained value of F_C is shown in parentheses. Therefore, this F_C can then be used for the simulation of the polymer dissolution and its roughness characteristics, which is the desired goal of this work.

Having validated our dissolution algorithm by comparison with published data and simulation results, the next step was to simulate the SR and LER behavior of the polymer

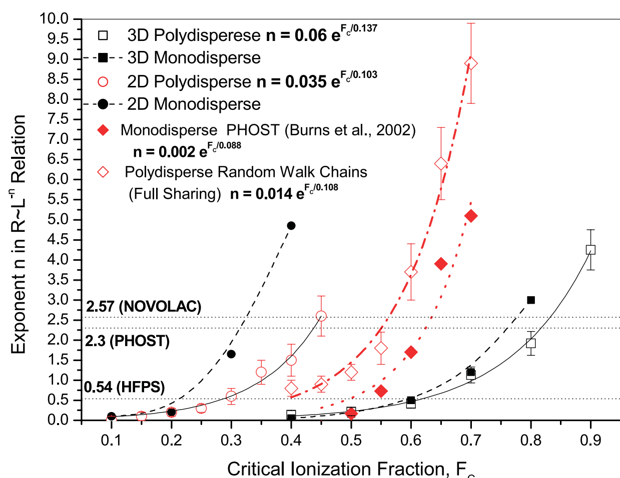

Fig. 6. Absolute values of the slope of $R(L,\langle L\rangle)$ curves from 2D and 3D simulations of both polydisperse and monodisperse chains, and comparison with corresponding simulations from Ref. [9]. Closer agreement regarding the steep slope increase, with the Burns et al. data is given by the full-sharing chain insertion [11]. The greater values are attributed to the difference in counting the chain-monomers between the two approaches. The horizontal dotted lines correspond to the slopes of the fits shown in Fig. 7 to the experimental data.

chains, under ideal exposure conditions (i.e. sharp, vertical square wave exposure) and without acid diffusion (i.e. all monomers deprotected in the exposure region)).

Fig. 8(a) shows the results from such 3D simulations, for average polymerization lengths of 10 and 20 monomers per chain and for $F_C=0.617$. As dissolution proceeds, SR increases, reaches a maximum and then decreases until the material completely dissolves. One should expect the final SR values to be 0 irrespective of the polymerization length. However, due to the chain stiffness and immobility in this model, during the last stages of dissolution, the chains that

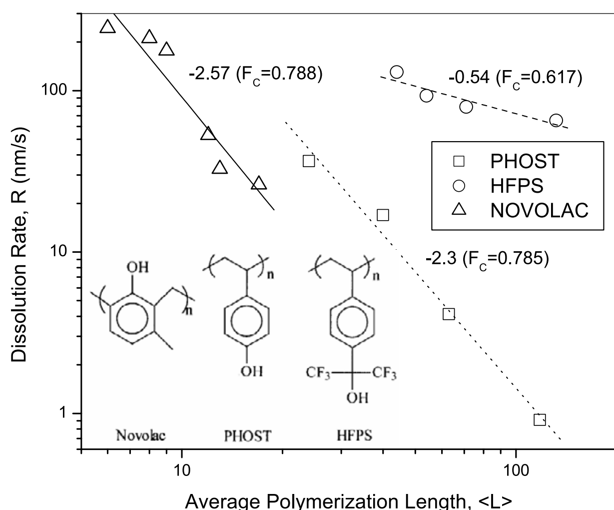

Fig. 7. Experimental dissolution rates. The corresponding slopes are shown and in parentheses are the values of F_C from the 3D simulations of the current work that result in the same slopes. This plot is created after data analysis of experimental results provided in [9].

are close or touch the bottom of the simulation domain are difficult to be ionized because it is not easy for the developer molecules to surround them. Therefore, dissolution is blocked and this is seen by the non-zero values of SR and by the changing slope towards the end of the dissolution time simulation of the normalized thickness curves. The phenomenon is more pronounced in higher polymerization lengths and is observed at lower dissolution cycles for higher values of critical ionization fraction. Also it is much more pronounced in the 2D case. Actually, for $F_C=0.785$, dissolution blocking is extremely pronounced as is seen in Fig. 8(b), where the normalized thickness and surface roughness (from 5 runs) are shown for $\langle L\rangle=10$. It is seen that in the 4 runs, dissolution is blocked with only about 50% of the film thickness removed. In one run, it was possible to dissolve almost 80% of the film. While such behavior can give a satisfactory slope by averaging the curves and taking a linear fit (shown in the figure by the straight line), and, therefore, resulting in the value of dissolution rate, it is inappropriate for giving a valid value of LER, because only a small fraction of the sidewall has been dissolved. This drawback is resolved with the introduction of the quasi-static version of the dissolution algorithm.

4. FAST (quasi-static) dissolution algorithm

The characteristics of the quasi-static dissolution algorithm have already presented in Section 2 and through Fig. 3. Summarizing, from the computational point of view its main characteristics are two. First, it uses a dynamic memory allocated linked list assigned to each polymer chain, therefore, accomplishes very fast search for specific chain locations in the polymer matrix. Second, it determines just after post-exposure bake the amount of deprotection each polymer chain carries and directly compares it with the critical ionization fraction, F_C (to be more accurate the combination of critical ionization and the ionization probability). If it is equal or greater, the chain is removed from the list and from the polymer matrix. This is done for all chains in a single cycle and not only for the chains that are in contact with the developer. Thus, the side-edge profile is delivered orders of magnitude faster and is as accurate as the dynamic one where only the chains in contact with the developer are dissolved if they satisfy the critical ionization fraction criterion.

Fig. 9(c) summarizes a quantitative comparison of the side-profiles obtained from the SLOW (dynamic) dissolution algorithm (Fig. 9(a)) and the FAST (quasi-static) (Fig. 9(b)). The distributions of side-surface positions obtained by the two algorithms are shown, for $F_C=0.5$ and $F_C=0.7$, for $\langle L\rangle=20$, and for a lattice of 50 nm in width, 50 nm in height and 300 in length. In the low F_C, both algorithms give essentially the same side profile, because dissolution blocking is not pronounced yet. However, while the SLOW algorithm takes 76 s to complete the FAST one

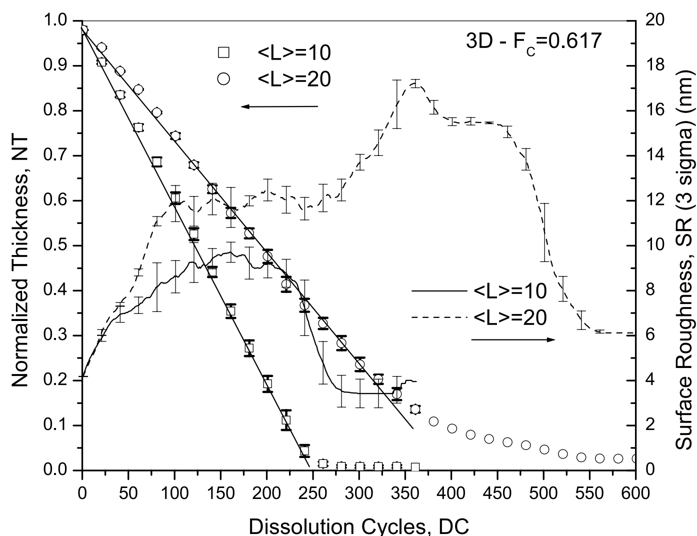

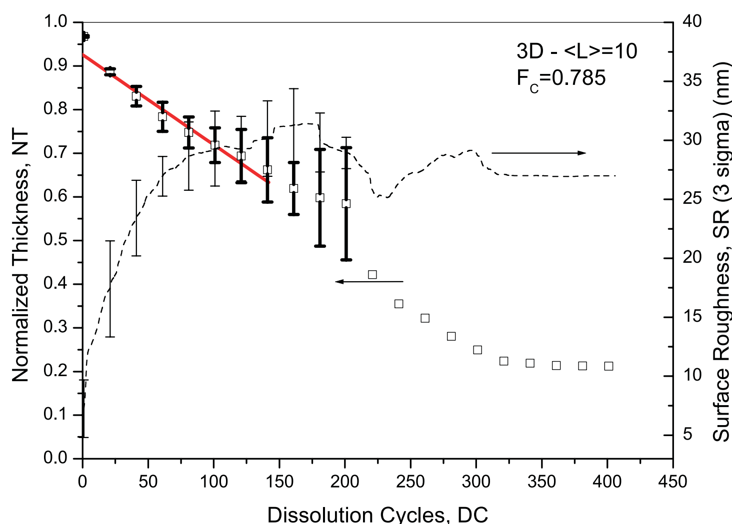

Fig. 8. 3D Simulation of the normalized thickness (NT) and surface roughness (SR) vs. dissolution cycles for (a) $\langle L\rangle = 10$ and 20, under ideal exposure conditions (i.e. sharp, vertical square wave exposure) and without acid diffusion (i.e. all monomers deprotected in the exposure region, without considering acid species diffusion). Dissolution blocking is pronounced in higher polymerization lengths and is seen by the change in slope of the otherwise linear curve of NT vs. DC. $F_C = 0.617$ (corresponds to HFPS). (b) Intense dissolution blocking for $F_C = 0.785$.

needs only 2 s. In the high F_C, the problems of dissolution blocking are revealed and the two distributions become noticeably different. With the SLOW algorithm, material residues are left near the bottom of the film due to dissolution blocking (Fig. 9(a)). This problem is diminished with the FAST dissolution algorithm (Fig. 9(b)). In this case the SLOW algorithm takes 321 s (Fig. 9(a)) and the FAST 4 s (Fig. 9(b)). The runs are performed on a Pentium IV 3.06 GHs laptop PC with 1 GB RAM. The gain in speed and most important in validity of the side-wall profile determination is important. Thus in order to determine dissolution rates and surface roughness evolution, the SLOW algorithm should be used while for LER studies the FAST one is appropriate.

One important aspect in LER quantification with the FAST dissolution algorithm is discussed now. Lets reconsider the 3D simulation of $\langle L\rangle = 10$ chains with $F_C = 0.5$ seen in Fig. 10(a). The figure actually shows the remaining chain sites after dissolution. At this point we are faced with a computational problem. Since, we want to

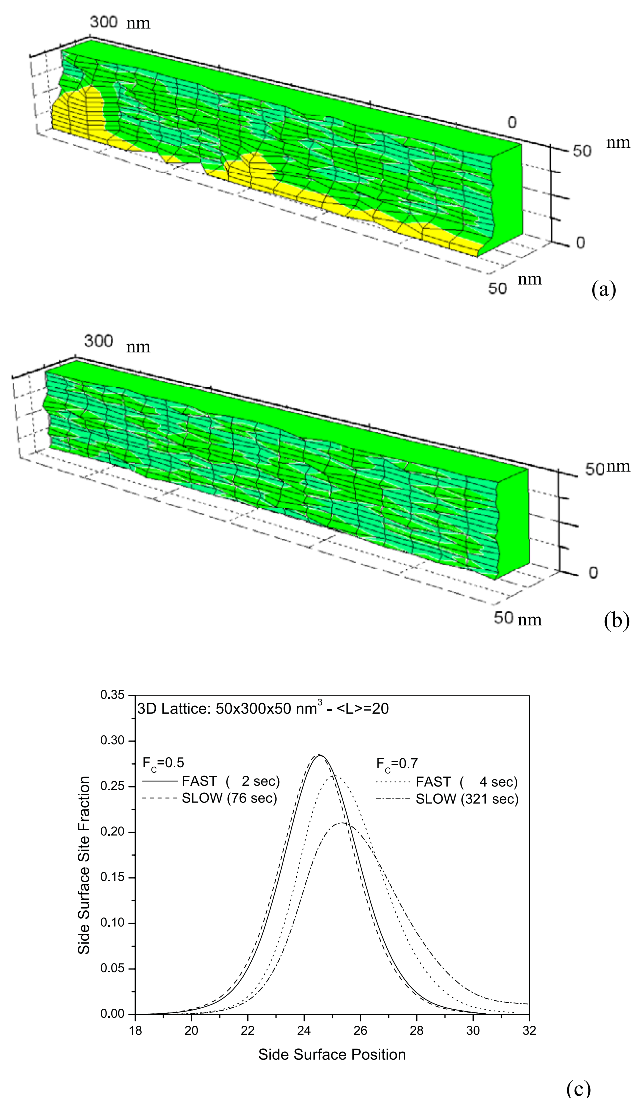

Fig. 9. Side-edge profile for (a) $F_C=0.7$ obtained from the SLOW (dynamic) dissolution algorithm. (b) $F_C=0.7$ obtained from the FAST (quasi-static) dissolution algorithm. Notice that the dynamics algorithm results in 'residues' due to dissolution blocking and hence in non-accurate LER evaluation. (c) Quantitative comparison between FAST and SLOW film dissolution algorithm for two values of $F_C=0.5$ and 0.7 and polydisperse chains with $\langle L \rangle=20$. In parentheses are the simulation times.

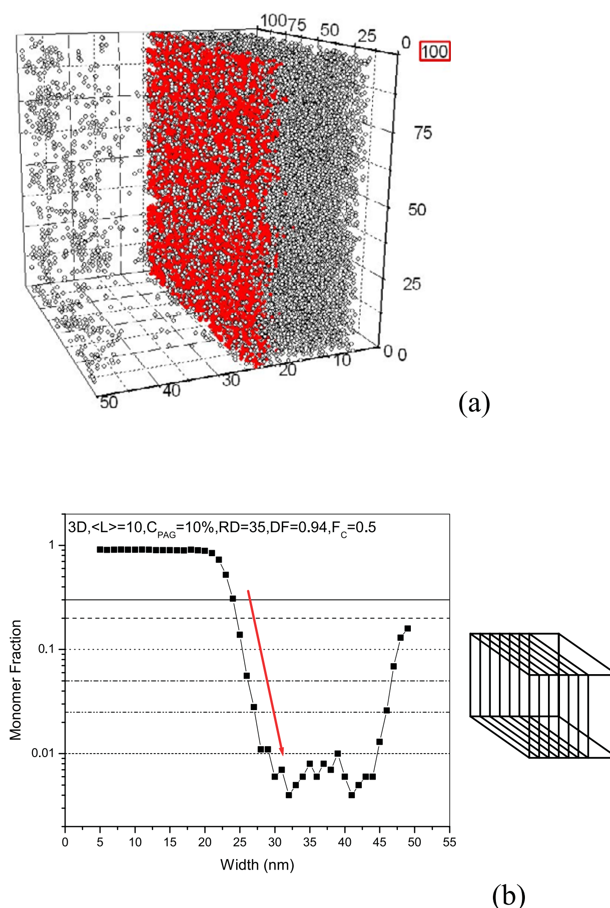

Fig. 10. (a). Remaining chains after dissolution with the FAST algorithm. The filled symbols represent sites that define the side edge. (b) Distribution of remaining monomers vs. width. This plot is used to determine the starting point for measuring LER. All monomers on its right are considered as swept away by the developer, even as they belong to chains not satisfying the F_C criterion. In this example this position ('rinse threshold') was selected to be at the 30% of non-dissolved sites, giving 25 nm as the starting point.

determine the side-profile coordinates, we should start from a point located in the exposed region where the material has been completely dissolved, and move towards the non-dissolved material recording the first non-dissolved monomer coordinate. This procedure should be performed for all the points on the sidewall. The problem is that in the dissolved region there are non-dissolved chains 'hanging' because they did not explicitly satisfy the dissolution threshold criterion, but were surrounded by chains, which dissolved. In addition there are parts of chains belonging to the non-exposed region but due to the periodic boundary condition in the horizontal direction, were extending to the opposite site of the lattice. One way to rinse away these chains is by percolation methods, however, this would add both complexity and time cost to the simulations. Thus, we prefer to use the following computational rinse method. The whole lattice is divided into slices of one lattice site in width and extending in the whole length and height. In each slice the non-dissolved monomer fraction is determined with respect to the number of sites in the slice, i.e. the slice surface. Fig. 10(b) shows the graph of this monomer fraction as we go from the non-dissolved to the dissolved region. In the transition region from the non-dissolved material to the dissolved, there is a steep decrease in the monomer fraction per slice. This is the region that the sidewall is formed. Progressing towards the lattice edge, the monomer fraction starts increasing again due to chains that are in the non-dissolved region but are extending in this side due to the horizontal boundary conditions. The trick now is to choose a rinse threshold in the monomer fraction and wash away lower fractions. This threshold will also define a width coordinate, which will be used as the staring point for

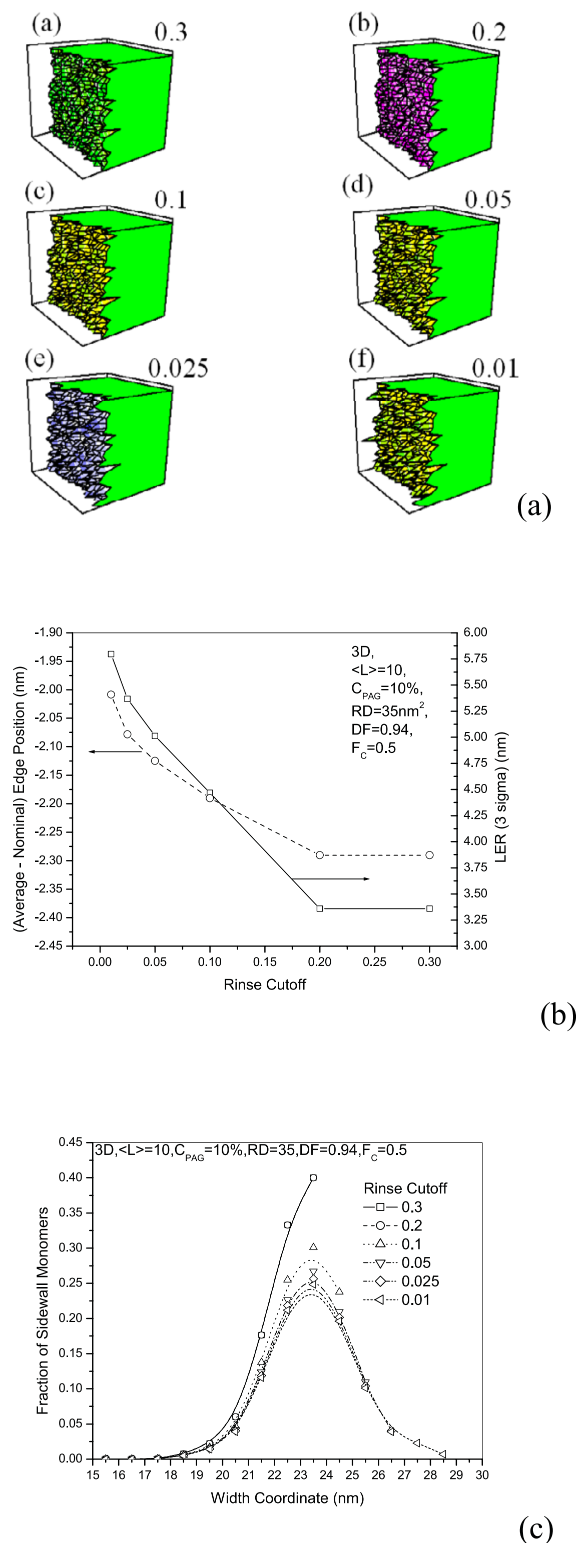

Fig. 11. (a) Sidewall profiles for various values of the rinse cutoff threshold. (b) Quantification of (Average–Nominal) edge position and LER vs. rinse threshold (c). Distribution of sidewall coordinates for the various rinse thresholds.

determining the sidewall coordinates as explained before. Examples of rinse thresholds are shown in Fig. 10(b) as horizontal lines intersecting monomer fractions at 0.3, 0.2, 0.1, 0.05, 0.025 and 0.01. The lower the selected rinse threshold the higher the expected sidewall roughness.

The sidewall profiles obtained for these rinse thresholds are shown in Fig. 11(a). Quantification of LER and average edge position is shown in Fig. 11(b). As the rinse threshold decreases LER increases from 3.25 nm towards 5.75 nm, while the quantity (Average − Nominal = 25 nm) edge position moves closer to 0 i.e. the edge position is found closer to the nominal.

The choice of rinse threshold seems somewhat arbitrary. However, it should be chosen to have such a value as to satisfy the fact that the sidewall positions show a Gaussian distribution. Fig. 11(c) shows the width coordinate distribution of the sidewall monomers for the rinse thresholds tested before. It is seen that as the rinse threshold decreases, the distribution tends more closely to the Gaussian one. In fact choosing 0.01 as the rinse threshold is the appropriate value in this case.

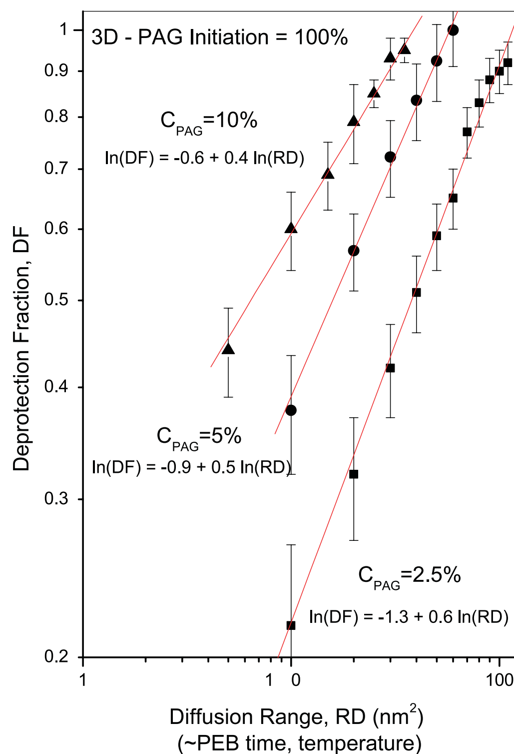

Fig. 12. Relation between simulated acid species diffusion range (RD) (which reflects the post-exposure temperature and/or time) and resulting deprotection fraction (DF) in 3D for $P_{INI}=1.0$ and different PAG concentrations. Diffusion length is approximately the square root of diffusion range. Notice in both graphs the departure from linearity due to lattice-size effects, when diffusion range increases.

5. Applications—effect of polymerization length (or molecular weight)

Chemically amplified resists are generally composed of a polymer matrix and a photosensitive compound (photo-acid generator, PAG). Upon exposure, PAG is initiated, produces acid species, which diffuse around the polymer matrix and induce deprotections on the monomers of the polymer chains. Thus, the more PAG sites are initiated the more acid is produced and the more deprotections will be induced, at a certain post-exposure bake temperature or diffusion range RD (i.e. the number of diffusion steps per initiated PAG site). The positions of the PAG sites are explicitly considered in the algorithm. Each one of them is characterized by an initiation probability P_{INI}, i.e. the probability that the specific site upon exposure will produce an acid site that can diffuse in the polymer lattice and create deprotections.

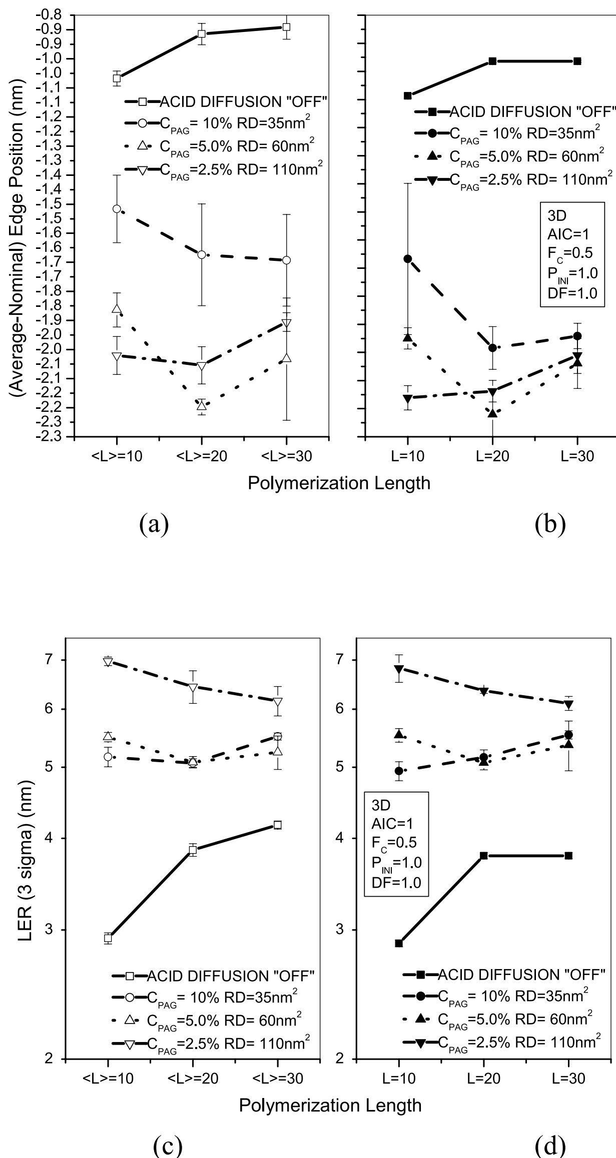

Fig. 13. Comparison of (Average–Nominal) edge position, (a) for polydisperse and (b) monodisperse chains with acid-diffusion 'off', and for (C_{PAG}=10%, RD=35 nm^2), (C_{PAG}=5%, RD=60 nm^2), (C_{PAG}=2.5%, RD=110 nm^2). Also the LER behavior under the same conditions for (c) polydisperse and (d) monodisperse chains.

In order to investigate in the simulation the effect of post-exposure bake temperature and/or time, we map these parameters to the diffusion range, RD. Greater RD means greater post-exposure bake temperature and time. We control the post-exposure temperature by controlling the RD in the simulations. However, the reaction probability was kept constant and equal to 1. This assumption can be relaxed of course. Deprotection fraction DF increases with acid diffusion range RD. This relation between the two is shown in Fig. 12 in log–log scale, for 100% PAG initiation and three PAG concentrations

The effect of 'diffusion-on' or '-off' and polymerization length for polydisperse and monodisperse chains, on average-nominal edge position and LER is shown in Fig. 13. Starting with the diffusion-off case it is clearly seen that (**1**) increasing polymerization length edge position moves closer to nominal (Fig. 13(a) and (b)) for both mono- and poly-disperse chains, (**2**) increasing polymerization length LER increases (Fig. 13(c) and (d)) for both mono- and poly-disperse chains.

For the acid-diffusion-on case, we work as follows: keeping DF constant at approximately 1.0 (i.e. all monomers in the exposure region are deprotected), it is seen from Fig. 12 that the values of the pair (C_{PAG}, RD) are, respectively, (2.5,110), (5, 60), (10, 35). Speaking in terms of (dose, post-exposure bake temperature/time), the previous pairs correspond, respectively, to (max, min), (medium, medium), and (min, max) conditions in order to have the same deprotection fraction in all of them. Simulations were performed with these parameter values. The results show that (**3**) edge position deviates more from the nominal compared to the diffusion-off case (Fig. 13(a) and (b)) for both mono- and poly-disperse chains, (**4**) the difference being analogous to decreasing PAG concentration or increasing diffusion range (Fig. 13(a) and (b)). For the pair (10, 35), the trend (2) also hold, however, the differences among the various polymerization lengths are less, (**5**) in absolute values, both LER and (Average–Nominal) edge position, are higher, (**6**) decreasing PAG concentration (therefore, increasing acid-diffusion range, in order to obtain the same DF, i.e. pair (5, 60)) the results become confusing, with approximately the same LER for all polymerization lengths, and (**7**) for pair (2.5, 110), LER clearly decreases with polymerization length increase.

Comparison between the polydisperse and monodisperse chains shows that (**8**) monodisperse chains deviate more from the nominal edge position (Fig. 13(a) and (b)), (**9**) monodisperse chains exhibit lower LER than the corresponding polydisperse (Fig. 13(c) and (d)), (**10**) polydisperse chains tend to result in more deviation from the nominal edge position, as polymerization length increases,

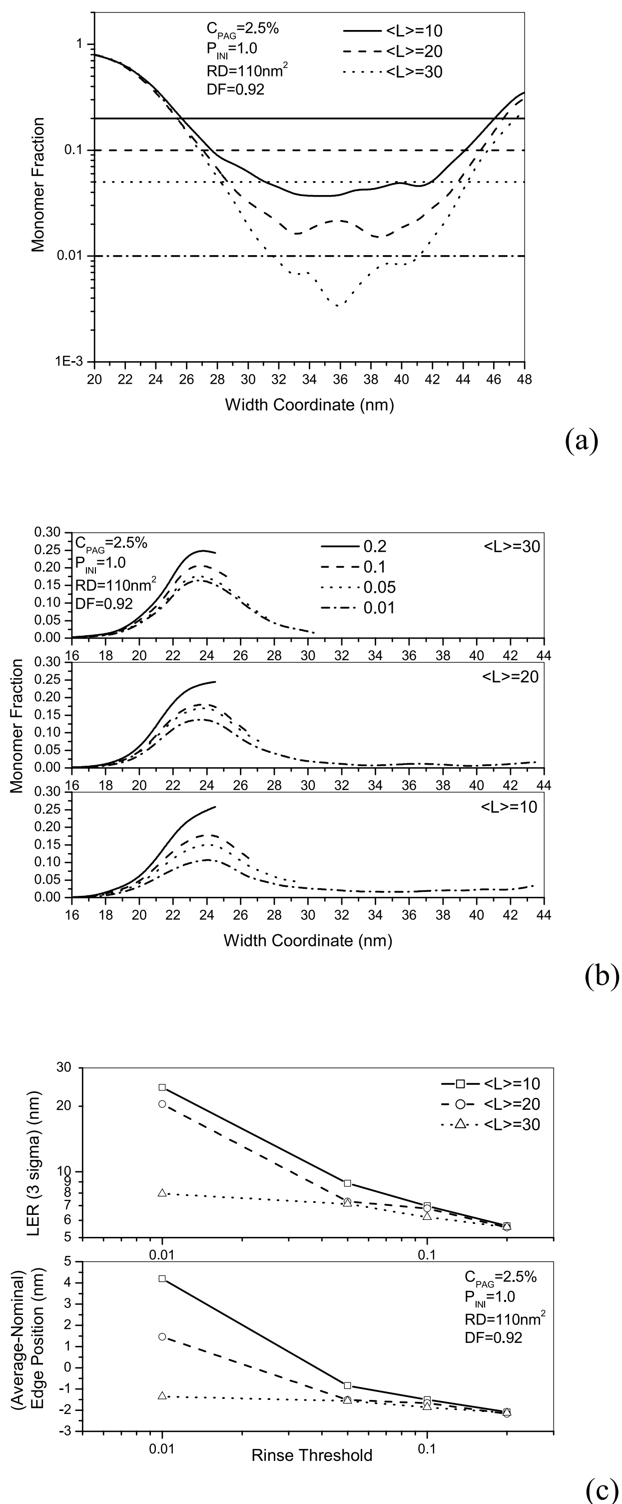

Fig. 14. One-run simulation for $\langle L \rangle = 10$, 20 and 30 at $C_{PAG} = 2.5\%$, for $RD = 110\ nm^2$, for rinse thresholds 0.2, 0.1, 0.05 and 0.01. (a) The monomer fraction vs. width coordinate. The sidewall for the $\langle L \rangle = 10$ chains is resolved only for thresholds greater than 0.05. (b) Rinse thresholds lower than 0.05 result in large negative skewness of the sidewall profile coordinate distribution for $\langle L \rangle = 10$, and 20. (c) Quantitative results for the effect of the rinse threshold one LER and (Average–Nominal) edge position. For thresholds larger than 0.05 there is very small dependence of the LER value upon the rinse threshold, while in any threshold the lines for each polymerization length do not cross.

when acid diffusion is 'off' or low. However, when the magnitude of acid diffusion is large (i.e. low PAG and high RD), then (**11**) polydisperse chains tend to result in less deviation from the nominal edge position, and (**12**) less LER, with polymerization length increase.

These observations are not an effect of the finite lattice size because larger lattices where also used, simulating much more chains in each polymerization length, and the effect was the same. Also, the runs were repeated for DF approximately 0.7, which result in average edge position closer to the nominal one, and the effect was still present and in fact the decrease of LER with increasing polymerization length was more pronounced (lower C_{PAG}, higher diffusion range cases). Finally, in order to be sure that this is not an effect of the rinse threshold, we performed runs for $\langle L \rangle = 10$, 20, and 30 at $C_{PAG} = 2.5\%$, for $RD = 110\ nm^2$, for rinse thresholds 0.2, 0.1, 0.05 and 0.01. The monomer fraction vs. width coordinate is shown in Fig. 14(a), where one observes that the sidewall for the $\langle L \rangle = 10$ chains is resolved only for thresholds greater than 0.05. Also from Fig. 14(b) it is seen that thresholds lower than 0.05 result in large negative skewness of the sidewall profile coordinate distribution for $\langle L \rangle = 10$, and 20. Quantitatively the effect of the rinse threshold is seen in Fig. 14(c). For thresholds larger than 0.05 there is very small dependence of the LER value upon the rinse threshold, while in any threshold the lines for each polymerization length do not cross. So it is best to use a rinse threshold of 0.1, and actually this is the value used in all the cases shown before.

Why does one observe this reverse size effect on LER at high diffusion ranges? The strong diffusion of acid species will create local deprotection sites in non-exposed regions. However, the local deprotection fraction is lower compared to the deprotection fraction in the main exposure volume. At a certain F_C, it is easier for the shorter chains to be dissolved and detached from the resist sidewall, thus increasing LER, than the longer chains for which the satisfaction of the critical ionization threshold criterion is more difficult.

6. Conclusions

Both a dynamic and a quasi-static molecular lever simulator for the dissolution of positive resist films were built. The development model was tested against its original version of the critical ionization model and an acceptable agreement between the two was found. The differences are attributed to the different chain insertion techniques used between the two models.

While the dynamic dissolution algorithm is appropriate for obtaining information about dissolution rate and surface roughness evolution, the dissolution blocking artifact and the increased computational time in high values of critical ionization fraction, make it inappropriate for LER studies. However, this is solved with the construction of a quasi-static dissolution algorithm, which is suitable for fast LER

quantification. It was based on the observation that given sufficient dissolution time, the final edge would be determined by the side chains in a thin side slice of the material between the completely exposed and non-exposed region. Using this algorithm it is possible to quantify the effect of critical ionization fraction, exposure dose, post-exposure bake temperature and acid-diffusion, and polymerization length on the final edge position and line-edge roughness. Results for the last two were shown.

The effect of the polymerization length for polydisperse polymer chains with Poisson distribution revealed that the LER decreases with decreasing polymerization length, only when no-acid diffusion is considered explicitly or when diffusion range is small into the unexposed region. Otherwise, acid-diffusion in high temperatures and/or times (that results in high deprotection fractions) tends to result in lower LER for longer polymers. This is attributed to the fact that at the extremes of the edge, the local deprotection fraction is low and in a certain critical ionization fraction, only the shorter chains are dissolved, thus causing increased roughness.

Acknowledgements

Financial support from European projects "CRISPIES" and "More Moore" as well as from INTEL is kindly acknowledged.

References

[1] Patsis GP, Gogolides E. Microelectron Eng 2001;57-58:563.
[2] Constantoudis V, Patsis GP, Tserepi A, Gogolides E. J Vac Sci Technol B 2003;21:1019.
[3] Constantoudis V, Patsis GP, Gogolides E. J Microlithogr Microfabrication Microsyst 2004;3:429.
[4] Patsis GP, Constantoudis V, Gogolides E. Microelectron Eng 2004; 75(3):297.
[5] Xiong S, Bokor J, Xiang Q, Fisher P, Dudley I, Rao P. Proc SPIE 2002;4689:733.
[6] Patterson K, Sturtevant JL, Alvis J, Benavides N, Bonser D, Cave N, Nelson-Thomas B, Taylor K. Proc SPIE 2001;4344:809.
[7] Patsis GP, Glezos N. J Vac Sci Technol B 2002;20:1303.
[8] Flanagin LW, Singh VK, Willson CG. J Polym Sci, Part: B 1999;37: 2103.
[9] Burns SD, Schmid GM, Tsiartas PC, Willson CG. J Vac Sci Technol B 2002;20(2):537.
[10] Schmid GM, Burns SD, Tsiartas PC, Wilson CG. J Vac Sci Technol B 2002;20(6):2913.
[11] Patsis GP. Math Comput Simulat 2005, in press.